Noise Scattering Study for a NACA 0012 Airfoil with a Shielding Flap

Florence V. Hutcheson[1], Christopher J. Bahr[1], Ian A. Clark[2]
NASA Langley Research Center, Hampton, Virginia, 23681
and
Daniel J. Stead[3]
Science and Technology Corporation, Hampton, Virginia, 23666

A flap (NACA 0015 airfoil or flat plate) is used for the shielding of noise scattered at the trailing edge of a NACA 0012 main airfoil. The effects of the shielding flap geometry and position relative to the main airfoil trailing edge, as well as the effects of sound source location and freestream flow, on shielding are examined. The sound source is a small plasma generated by a high-energy laser beam focused to a point. In-flow microphone measurements are acquired in the midspan plane of the test model over a broad range of streamwise stations, and shielding levels are calculated over different frequency ranges from the measurements acquired with and without the model installed. Compared to the shielding levels provided by the isolated main airfoil, the shifted-flap configurations are shown to be more effective in increasing shielding than the gapped configurations. The flat and sharp-edge geometry of the plate is also shown to be a more effective shielding element than the NACA 0015 airfoil. Finally, shielding below and upstream of the main airfoil is shown to decrease in the presence of flow, with generally more pronounced effects observed with the shielding flap installed.

I. Introduction

Aircraft propulsion noise shielding, wherein engines can be placed above an aircraft wing or fuselage to partially block acoustic radiation toward ground-based observers, is an aircraft design approach that can be used to reduce the community noise impact of commercial aviation. This approach to noise reduction has been the subject of growing interest,[1-5] which has revealed a need for further validation and improvement of current noise scattering prediction tools. To address this need, a NATO task group led by NASA and DLR representatives established an experimental database for the validation of computational methodologies. The effort included the execution of dedicated noise scattering tests using a common airfoil design as the scattering surface and a well-defined, laser-induced, sound source. One of these dedicated noise scattering tests was conducted at the NASA Langley Research Center and is detailed in Ref. 6. The noise scattering surface was a simple NACA 0012 airfoil, and the effects of flow and relative source location on shielding were evaluated. In a follow-on effort, which is the subject of this paper, the noise scattering database was expanded to include acoustic measurements from a more complex scattering geometry. A small flap was added to the trailing edge of the NACA 0012 airfoil, and the effect of its relative placement and geometry on noise shielding was examined. In addition to expanding the noise scattering database available to NASA prediction tools, this scattering test also supports the development of a noise reduction concept presented in a companion paper.[7] In that paper, the potential of the flap (also referred to as the shielding flap) as a noise reduction device applicable to a NATO MULDICON vehicle[7] is evaluated. Together with the NASA PAASc scattering prediction method,[8] the experimental study presented here was used for the initial exploration and development of the shielding flap concept.

The test setup, data acquisition procedures and sound source characteristics are presented in the first part of this paper. These are followed by an examination of the effects on shielding of the flap position and geometry, flow and source location. The paper concludes with a summary of the study.

---

[1] Senior Research Engineer, AIAA Associate Fellow
[2] Research Engineer, AIAA Senior Member
[3] Test Engineer

II. Experimental Setup

The experiment was conducted in NASA Langley Research Center's Quiet Flow Facility (QFF). The QFF is specifically designed for aeroacoustic testing. Its test chamber is equipped with a 0.61 by 0.91 m rectangular open-jet nozzle. Side plates are attached to the short sides of the nozzle while the 0.91 m sides of the test section remain open. The flow circuit employs baffles, turbulence screens and turning vanes to ensure a quiet, low-turbulence air flow from the open jet. Flow speeds up to a Mach number of 0.17 can be obtained. The anechoic room (7.3 m wide by 9.2 m long by 6.1 m high) is lined with acoustically absorbent wedges, 91.5 cm deep, to provide an essentially acoustic-reflection-free environment for acoustic measurements down to about 70 Hz.[9] The room is also constructed with a 91.5 cm air space between double walls and is mounted on springs to isolate it structurally from the remainder of the building and thus minimize the transmission of structure-borne noise arising from other parts of the facility.

The test setup, shown in Fig. 1, was similar to that used in a previous experiment.[6] The test model, which consists of a main airfoil (NACA 0012) with a shielding flap (not shown), was positioned at the center of the test section with each end of the test articles mounted to the test section side plates. A 0.3175 cm (1/8") Type 4138 Brüel & Kjær microphone equipped with a GRAS RA0173 nosecone and mounted on a linear traverse was used to acquire the acoustic measurements inside the test section at different streamwise stations and flow conditions.

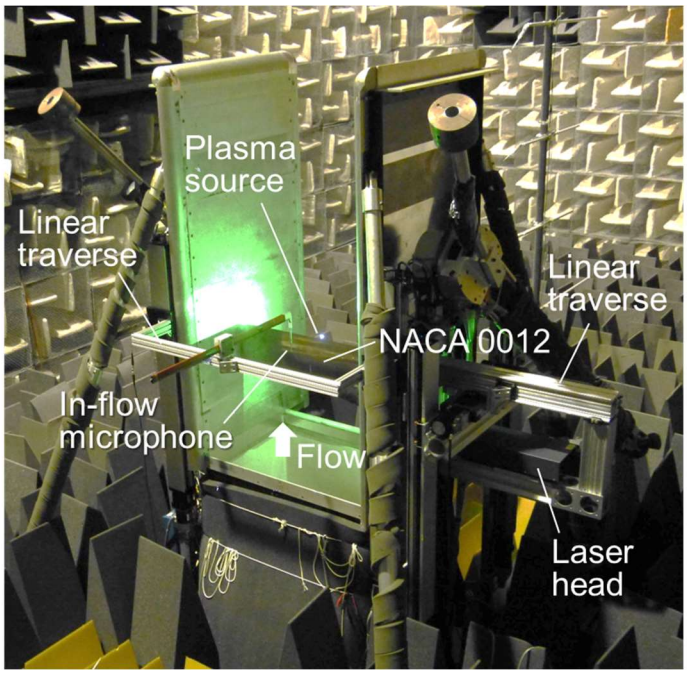

Fig. 1 QFF experimental setup.

The sound source was a laser-induced plasma that, once formed, rapidly expanded to generate a nearly omnidirectional pressure wave that propagated as an isentropic acoustic wave in the far field. The small plasma was generated by a pulsed Nd:YAG Gemini PIV laser focused to a point in the test section. This laser system has a pulse energy of 120 mJ with a wavelength of 532 nm and a pulse width of 3 to 5 ns. As depicted in Fig. 2, the laser system was positioned behind one of the test section walls (which was modified to incorporate a 0.95 cm-thick tempered glass window), and a set of 7.62 cm-diameter achromatic expansion, collimating, and focusing lenses was used to focus the laser beam at the test section midspan.

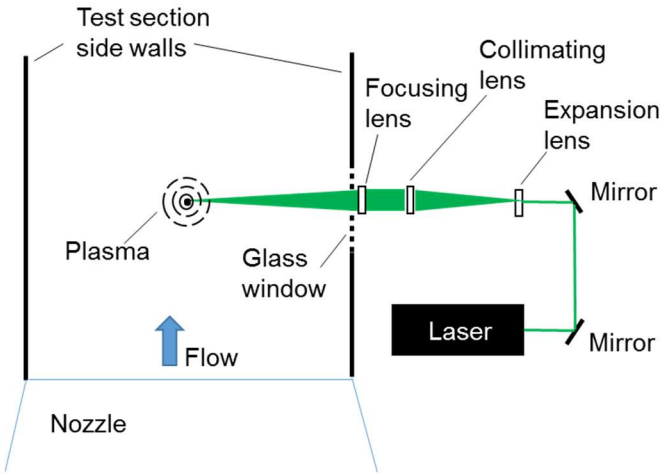

Fig. 2 Sketch of laser and optical lens setup.

To minimize laser reflections, the path of the laser beam from the laser head to the test section wall window was encased by installing tubes between the optical lenses and between the focusing lens and the test section wall window (see Fig. 3). A photodetector was also positioned near the laser window to record the plasma (sound source) occurrences.

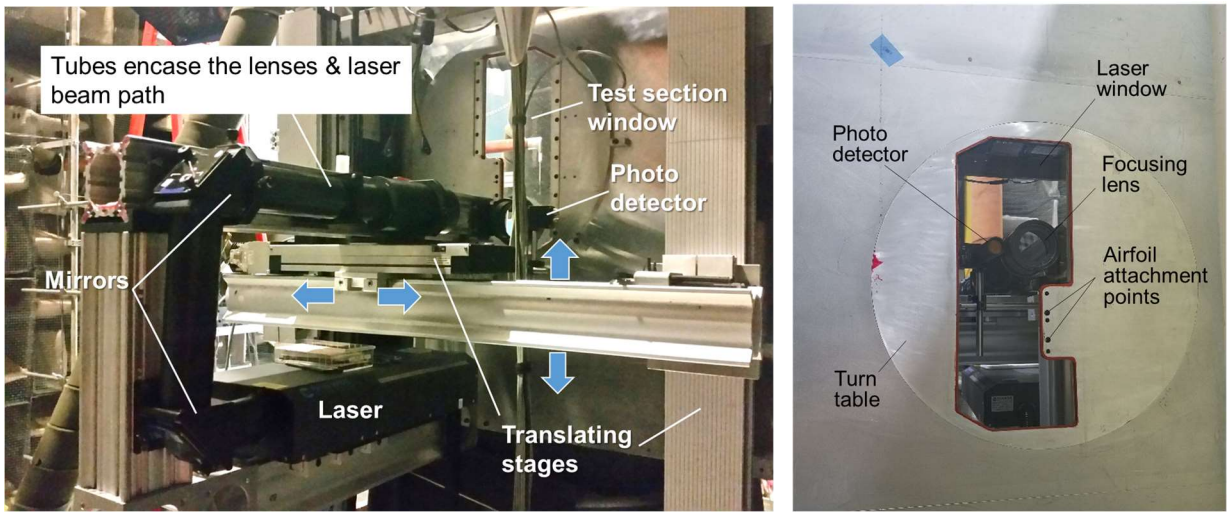

(a) **(b)**

Fig. 3 Laser and optical lens assembly; (a) view from behind the test section wall; (b) view from inside the test section.

The traverse system used to position the in-flow microphone and the laser/optic assembly (shown in Figs. 1 and 3a) was designed to be compact and rigid in order to minimize flow-induced vibrations. It was used to traverse the in-flow survey microphone in the streamwise direction and the laser system assembly in both streamwise and crosswise directions to position the sound source at chosen locations. The motors of the traverse system were turned off during the acquisition of each data point to avoid acoustic and/or electronic contamination.

III. Test Model Configurations, Data Acquisition and Processing

Schematics of the test setup and model configuration are shown in Fig. 4. The NACA 0012 main airfoil was installed in the test section at 0˚ angle-of-attack, and a NACA 0015 airfoil (shielding flap) was installed in the trailing edge region of the NACA 0012. The chord of the NACA 0012 was 200 mm. Several shielding flap configurations were evaluated by varying the chord, shift, overhang and deflection angle of the flap as listed in Table 1. Referring to Fig. 4, positive overhang values correspond to configurations where the leading edge of the shielding element is upstream of the trailing edge of the main airfoil, and negative deflection angles are achieved when the trailing edge of the shielding element is deflected toward the sound source. Additional configurations were tested where the NACA 0015 airfoil was removed and replaced with a 0.254 mm-thick flat plate of matching chord. The main airfoil and shielding flaps (NACA 0015 airfoil and flat plate) had a span of 0.91 m that extended through the full width of the test section. While the surface of the flat plate remained untripped, thin strips of serrated tape (0.127 mm thick) were placed along the span of the NACA 0012 and 0015 airfoils to trip the boundary layer and induce its transition to a turbulent state. The strips were positioned at 5% chord on the main airfoil and at approximately 10% chord on the flap.

The microphone measurements were acquired in the midspan plane of the test model, one chord away (200 mm) from the NACA 0012 chordline. The survey microphone was traversed in the streamwise direction, up to 200 mm upstream and 400 mm downstream of the main airfoil leading edge, while the sound source (laser-induced plasma) was positioned on the opposite side of the airfoil, in the trailing-edge region. Each set of in-flow (survey) microphone measurements was acquired with and without the test model installed (i.e., for shielded and unshielded conditions). The sound source was positioned at 70%, 75% and 100% chord of the main airfoil (corresponding to streamwise locations x = 140, 150 and 200 mm, respectively). When positioned at 75% and 100% chord, the source was at a normal distance of 25 mm from the airfoil surface, while, when positioned at 70% chord, the source was at a normal distance of 40 mm from the airfoil surface. The microphone surveys were performed for three flow speeds (Mach numbers of 0, 0.13 and 0.16) for the NACA 0015 airfoil flap configurations, as well as for a configuration where the flat plate was used as an extension of the main airfoil trailing edge (see Section V). Measurements were only acquired without flow for the rest of the flat plate flap configurations tested.

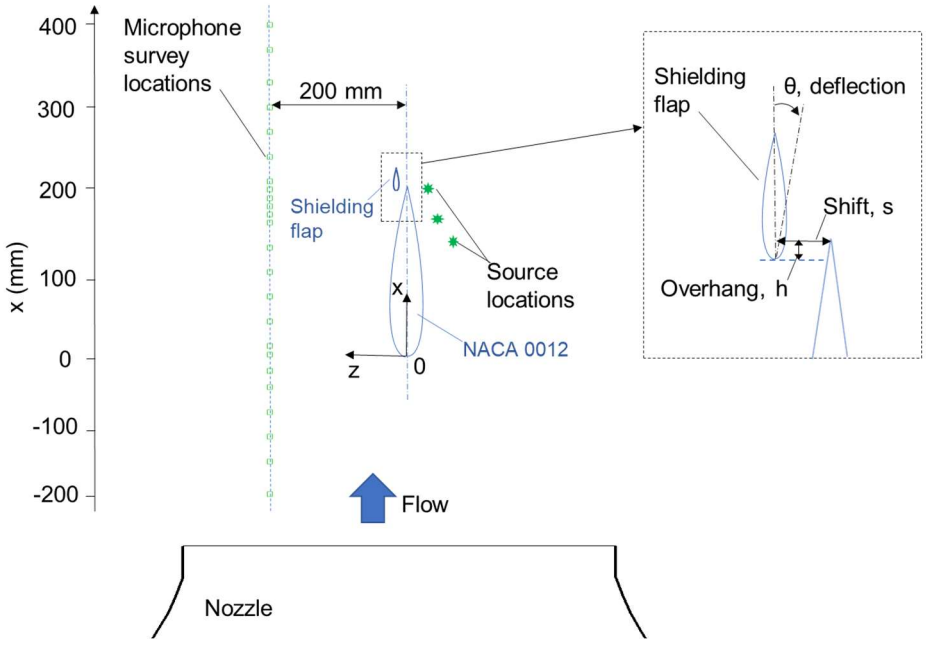

Fig. 4 Schematic of test setup with microphone survey and sound source locations.

Table 1. Model configurations and parameter variation.

Shielding element	Chord (mm)	Shift, s (mm)	Overhang, h (mm)	Deflection, θ (deg.)
NACA 0015	**25.4; 50.8**	**0; 12.7; 19.05**	**6.35; 0; -6.35; -12.7**	**-10; 0; +10**
Flat Plate	**25.4; 50.8**	**0; 19.05**	**6.35; 0; -6.35; -12.7**	**-10; 0; +10**

The sound source was generated with a repetition rate of 10 Hz, and the survey microphone signal was recorded for 30 s. This created time records of 300 acoustic pulses per data point. The survey microphone data were acquired with a sampling rate of 1.25 MSamples/s. An analog highpass filter was set at 250 Hz and the lowpass antialiasing filter was set at 500 kHz. For the processing of each data point acquired, the time signal was gated with 25% Tukey windows to isolate the portions of the signal that corresponded to the sound that was directly propagating from the source or to the scattered sound that was propagating from the main airfoil and shielding flap leading and trailing edges. This gating rejected reflections from facility surfaces, mitigated facility background and model airframe noise, and retained the portions of the time signal that contained the acoustic pulses of interest. Finally, mean-squared averaged spectra were obtained using data blocks that were zero-padded to the number of samples needed to obtain a frequency resolution of 61 Hz.

The last step in the processing of the acquired test data is the calculation of the frequency-integrated shielding levels, $\gamma_p^n(f_c)$ and $\gamma_p^n(\infty)$, where

$$\gamma_p^n(f_c) = 20\ log_{10}(\eta^n(f_c)) \tag{1}$$

is the octave band normalized shielding level, which is calculated over octave bands of center frequencies, f_c = 7, 14 and 28 kHz, respectively, and

$$\gamma_p^n(\infty) = 20\ log_{10}(\eta^n(\infty)) \tag{2}$$

is the overall normalized shielding level. In Eqs. (1) and (2), $\eta^n(f_c)$ and $\eta^n(\infty)$ are, respectively, the octave band and overall shielding factors, which are defined as

$$\eta^n(f_c) = \left[\frac{\sqrt{2}}{f_c} \int_{f_c/\sqrt{2}}^{f_c\sqrt{2}} \eta^2(f)\ df\right]^{1/2} \tag{3}$$

and

$$\eta^n(\infty) = \left[\frac{1}{(f_u - f_l)} \int_{f_l}^{f_u} \eta^2(f)\ df\right]^{1/2}, \tag{4}$$

where $f_u = \sqrt{2} * 28$ kHz, $f_l = \frac{1}{\sqrt{2}} * 7$ kHz and

$$\eta^2(f) = p_s^2(f)/p_i^2(f). \tag{5}$$

In Eq. (5), p_i is the acoustic pressure from the isolated source field (i.e., test model removed), and p_s is the acoustic pressure from the scattered field (i.e., test model installed). Note that the overall frequency range, octave bands and shielding quantities defined above were chosen to be consistent with those used in the analysis of the data acquired in the noise scattering test performed previously in the QFF on the isolated NACA0012 airfoil.[6] However, unlike in Reference 6, the shielding level calculations here are limited to a frequency range of 5 to 40 kHz, as the nosecone used on the survey microphone showed a sharp response cutoff at 40 kHz and higher frequencies. This frequency cutoff was later determined to be caused by a damaged screen inside the nosecone.

IV. Sound Source Characteristics

A. Sound source repeatability

Data recorded from fixed microphones installed both flush with the test section wall and outside of the test section were used to monitor and verify the repeatability of the acoustic pulse generated by the laser-induced sound source throughout the test. Brüel & Kjær Type 4138 microphones with protective gridcaps removed were installed along an unobstructed path from the sound source and sufficiently far away from other hardware to isolate the waveform of the sound source from secondary reflections. The averaged waveforms produced by the sound source and measured by the microphone outside of the test section for data points acquired without flow at the beginning and around the middle of the test campaign are shown in Fig. 5. Note that these waveforms are aligned to account for the speed of sound difference in the facility from one date to another. The signal waveforms shown are representative of the range of very small variations observed over the span of the test and demonstrate the repeatability of the sound source produced by the laser system.

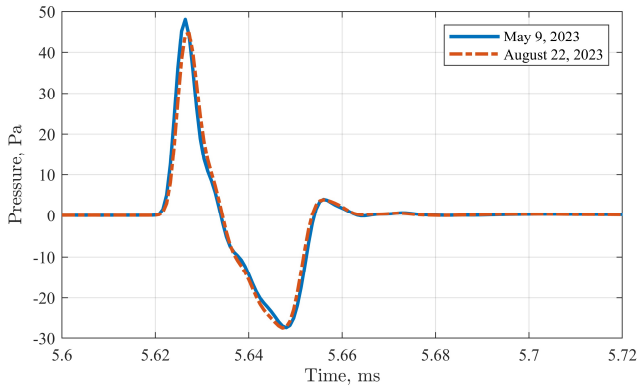

Fig. 5 Laser-induced sound source waveform repeatability.

B. Sound source directivity

Prior to the start of the test and as part of a separate study,[10] acoustic measurements of the isolated sound source were obtained from microphones distributed around and pointed at the source location, 1.67 m away, along two polar arcs with 0° polar angle corresponding to the downstream direction. The first arc of microphones was positioned in the midspan plane of the test section, corresponding to the plane of the traversing microphone in this study, and the other was offset spanwise at a 30° azimuthal angle from the midspan plane. The protective gridcaps of the microphones were removed to reduce installation effects on the measured signals, and the resultant spectra shown in Fig. 6 for data without flow were corrected for atmospheric attenuation, the approximate normal-incidence free-field response of the microphones, and the microphone actuator response. The collapse of the spectra seen in this figure is consistent with the expected omnidirectional ("monopole-like") character of the laser-induced sound source. The effect of flow on the sound source is discussed in Section V.D.

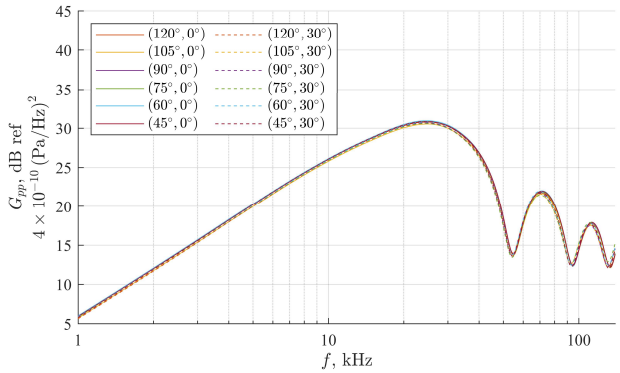

Fig. 6 Sound source energy spectral densities, G_{pp}, for polar arcs at two azimuthal angles; no flow.

V. Test Results

The effects of the shielding flap (airfoil or plate) placement, source location and flow were examined, and the results obtained for a representative subset of the configurations tested are presented in this section. These configurations are listed in Table 2.

Table 2. Model configuration description

Configuration	Shielding flap	Flap chord (mm)	Shift, s (mm)	Overhang, h (mm)	Deflection, θ (deg.)
#1 Isolated main airfoil 	None	N/A	N/A	N/A	N/A
#2 Extension plate 	Plate	25.4	0	0	0
#3 Gapped plate 	Plate	25.4	0	-6.35	0
#4 Shifted plate with overhang 	Plate	25.4	19.05	+6.35	0
#5 Gapped airfoil 	Airfoil (NACA 0015)	25.4	0	-6.35	0
#6 Shifted airfoil with overhang 	Airfoil (NACA 0015)	25.4	19.05	+6.35	0
#7 Shifted airfoil with overhang 	Airfoil (NACA 0015)	25.4	12.7	+6.35	0
#8 Shifted airfoil w/o overhang 	Airfoil (NACA 0015)	25.4	12.7	0	0
#9 Shifted & deflected airfoil with overhang 	Airfoil (NACA 0015)	25.4	12.7	+6.35	-10
#10 Shifted & deflected airfoil w/o overhang 	Airfoil (NACA 0015)	25.4	12.7	0	-10

A. Results presentation

As in Ref. 6, microphone free-field corrections and atmospheric absorption corrections were not applied in the calculation of the shielding quantities presented here. Although these corrections could be quantified for the isolated source test cases, the multipath nature of the signal received at the microphone once the main airfoil and shielding flap are installed complicated this process. Note that except for the case of the isolated main airfoil with the source positioned at 100% chord, there was not a direct line of sight between the sound source and the microphone survey locations for any of the other model configurations tested. Depending on the configuration, the microphone received sound from two or more paths: the sound that was scattered at the leading and trailing edges of the main airfoil, the sound that was scattered at the leading and trailing edges of the shielding flap, and the sound that propagated through the gap between the main airfoil and shielding flap. Except in some instances for the sound scattered from the main airfoil leading edge, the respective portions of the time signal corresponding to the sound scattered through the different paths cannot be separated, which is required to apply these corrections. The error on the calculation of the shielding quantities (Eqs. 1 through 5) associated with omitting these corrections is estimated to be less than 1 dB, based on angle of incidence range and distances involved for atmospheric attenuation.

The gated time signals obtained at microphone survey location x = 200 mm (main airfoil trailing edge streamwise location) for model configurations #1 (isolated main airfoil) and #6 (main airfoil with shifted and overhung shielding flap) are shown in Fig.7. The source is at the 70% chord position and the flow Mach number is 0. The peaks corresponding to the noise that propagates from the leading and trailing edges of the main airfoil in configuration #1 are easily identified. With the flap installed, the direct line of sight between the main airfoil trailing edge and the microphone is blocked by the flap. Although the smaller peak associated with the sound scattered from the main airfoil leading edge remains nearly unchanged, the large peak associated with scattering from the main airfoil trailing edge in configuration #1 is replaced with a set of smaller peaks; the first two, based on distance and travel time, corresponding to the noise scattered from the flap leading and trailing edges. The other peaks in the set could be partly attributed to the scattering of reflections between the flap and the main airfoil surfaces.

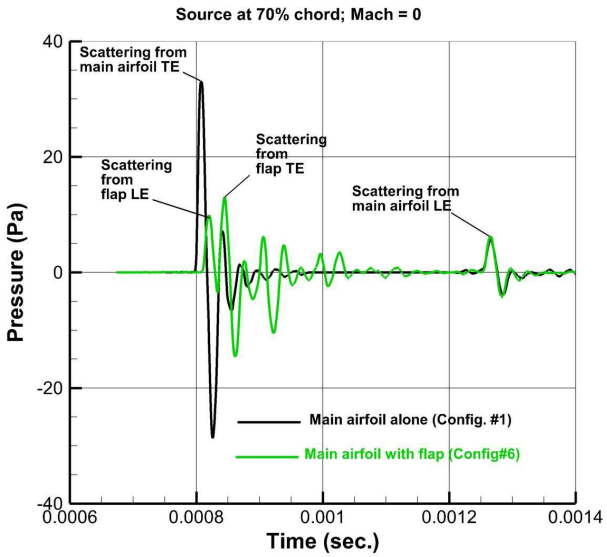

Fig. 7 Gated time signals for configurations #1 and #6. Source at 70% chord; no flow.

The narrowband shielding spectra obtained for model configuration #6 by subtracting the model-installed and empty test section spectra at four microphone survey locations are displayed in Fig. 8(a). It is seen that the multipath nature of the acoustic signals leads to interference patterns that can vary significantly with frequency and observer location. Thus, at x = 160 mm and 170 mm, maximum shielding levels occur between 10 and 20 kHz with local maxima (large negative peak) at 15 kHz and 10 kHz, respectively. At x = 210 mm, maximum shielding occurs above 20 kHz, while at the most downstream survey location, x = 400 mm, shielding levels remain around -10 dB over the full frequency range. This sensitivity to changes in frequency and observer location makes it difficult to capture and

assess the overall effects of a given model configuration on shielding. The calculation of integrated shielding levels is intended to facilitate that process. Thus, the shielding levels obtained for the same model configuration and integrated over three frequency ranges, namely 5 to 10 kHz, 10 to 20 kHz and 20 to 40 kHz (corresponding to octave bands of center frequencies, 7, 14 and 28 kHz, respectively) are shown in Fig. 8(b) along with shielding levels integrated over the full frequency range (5 to 40 kHz). Data point locations are indicated by small circular symbols along these curves. It is seen that the integrated levels properly reflect the zones and frequency ranges of increased shielding, as well as the shielding peak locations seen in Fig. 8(a). Integrated shielding levels are used in the rest of this paper to show the overall effects of configuration changes on shielding.

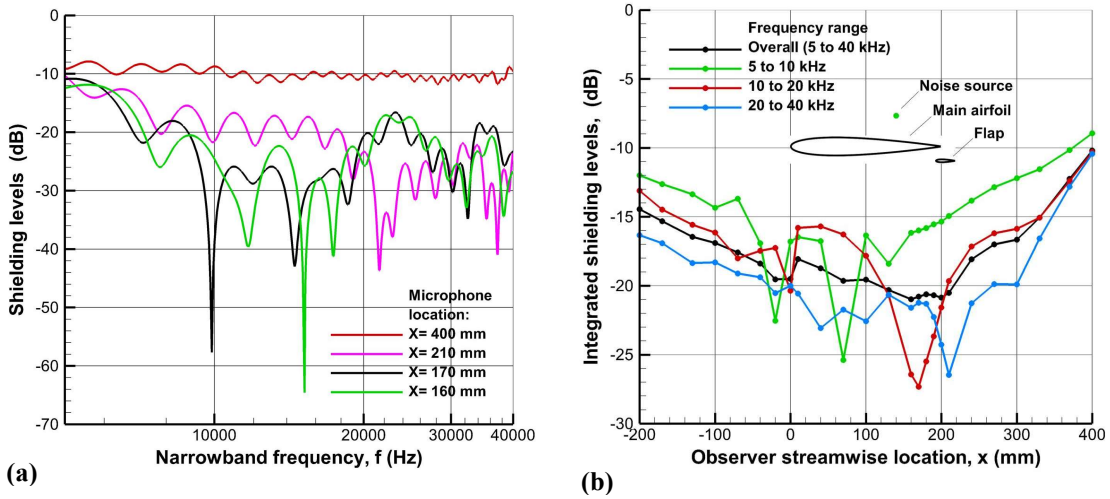

Fig. 8 (a) Narrowband shielding spectra; (b) Integrated shielding levels. Model configuration #6; source at 70% chord; no flow.

B. Effect of shielding element geometry and placement

The integrated shielding levels obtained for configuration #1 (isolated main airfoil) are compared to those obtained for configurations #2 (extension plate), #3 (gapped plate) and #5 (gapped airfoil) in Fig. 9. The source is positioned at 70% chord, and the flow Mach number is 0. With configuration #2, which effectively extends the chord of the main airfoil and shifts the trailing edge diffraction further downstream, the largest increase in shielding is observed at microphone locations that are downstream of the main airfoil leading edge, where the sound field is dominated (or largely affected) by trailing edge diffraction. In the region upstream of the airfoil, the added shielding provided by the extension plate decreases as scattering from the leading edge becomes dominant.

For configuration #3, the plate is moved in the downstream direction to create a 6.35 mm gap between the main airfoil trailing edge and the plate leading edge. It is seen in Fig. 9(a) that compared to the results obtained with the isolated main airfoil, the gapped plate leads to an increase in noise at most microphone locations. The first exception to this is at the most upstream locations, where scattering from the main airfoil leading edge likely dominates (and shielding levels approach those of the isolated main airfoil). The second exception is at the most downstream locations, where shielding is increased. For this gapped plate configuration, the measured sound field results not only from diffraction at the main airfoil leading and trailing edges, but also from diffraction at the plate leading and trailing edges and secondary scattering of these diffracted signals from the airfoil and flap surfaces. This may contribute to the increase in noise observed in the region near and upstream of the main airfoil trailing edge. The corresponding integrated shielding levels obtained for each octave band are shown in Figs. 9(b), (c) and (d), respectively. It is seen in these figures that each displays a zone of significantly increased shielding downstream of the main airfoil, and that this zone shifts further downstream with increase in frequency. It is seen as well that the region of increased noise extends over a broader range of survey locations as frequency increases. Similar results (not shown) were obtained

when doubling the gap size, only with an increase in noise over an even broader range of observer locations and with the zones of increased shielding shifted further downstream (and maximum shielding levels reduced).

When the plate is replaced with the airfoil (configuration #5), a small decrease in shielding is observed at most survey locations (compared to that achieved with the plate). This decrease in performance may be attributed to increased scattering and reflections from the rounded leading edge of the airfoil[11] (as opposed to the sharp leading edge of the plate). The difference in the shielding levels provided, respectively, by the plate and airfoil was also found to be accentuated when doubling the gap size (results not shown). The airfoil configuration performed significantly worse than the plate, as there was a difference in shielding levels of approximately 2 to 3 dB between the two configurations at most observer locations.

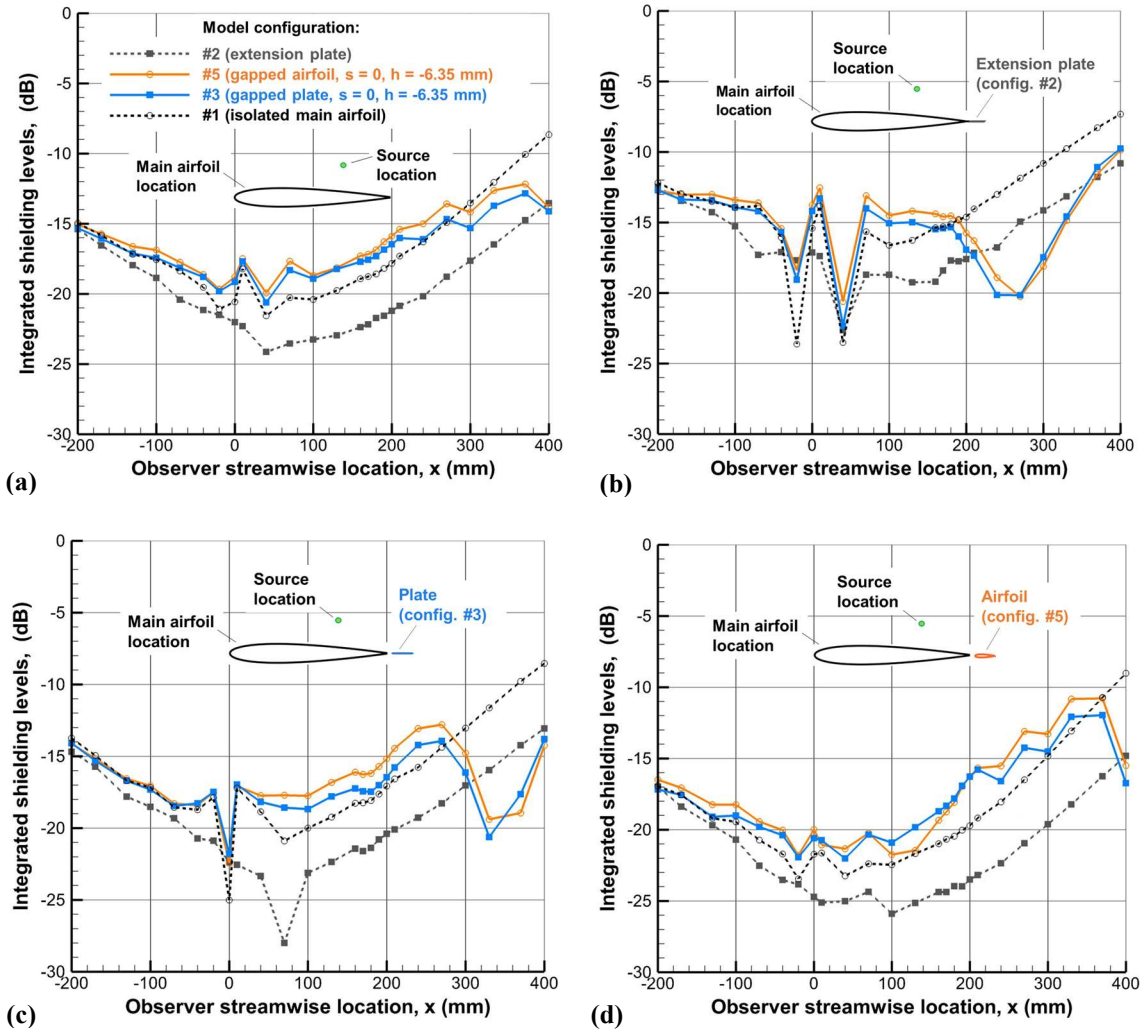

Fig. 9 Integrated shielding levels for configurations #1 (isolated main airfoil), #2 (extension plate), #3 (gapped plate) and #5 (gapped airfoil). Source at 70% chord; no flow. (a) 5 to 40 kHz; (b) 5 to 10 kHz; (c) 10 to 20 kHz; (d) 20 to 40 kHz.

The integrated shielding levels obtained when the plate (configuration #4) and airfoil (configuration #6) are shifted toward the microphones and slightly upstream of the main airfoil trailing edge are shown in Fig. 10 and compared again to those obtained with the isolated main airfoil and extension plate. Configurations #4 and #6 are seen to perform better than their gapped counterparts. They show little to no decrease in shielding below the main airfoil and shielding levels close to those achieved with the extension plate downstream of the airfoil midchord. For

these configurations, the shielding flap blocks the direct path between the main airfoil trailing edge and microphone locations that are approximately downstream of the main airfoil midchord. This at least partially shields these locations from the main airfoil trailing edge diffraction. It is also seen in Fig. 10 that, as with the gapped configurations, the plate performs better than the airfoil.

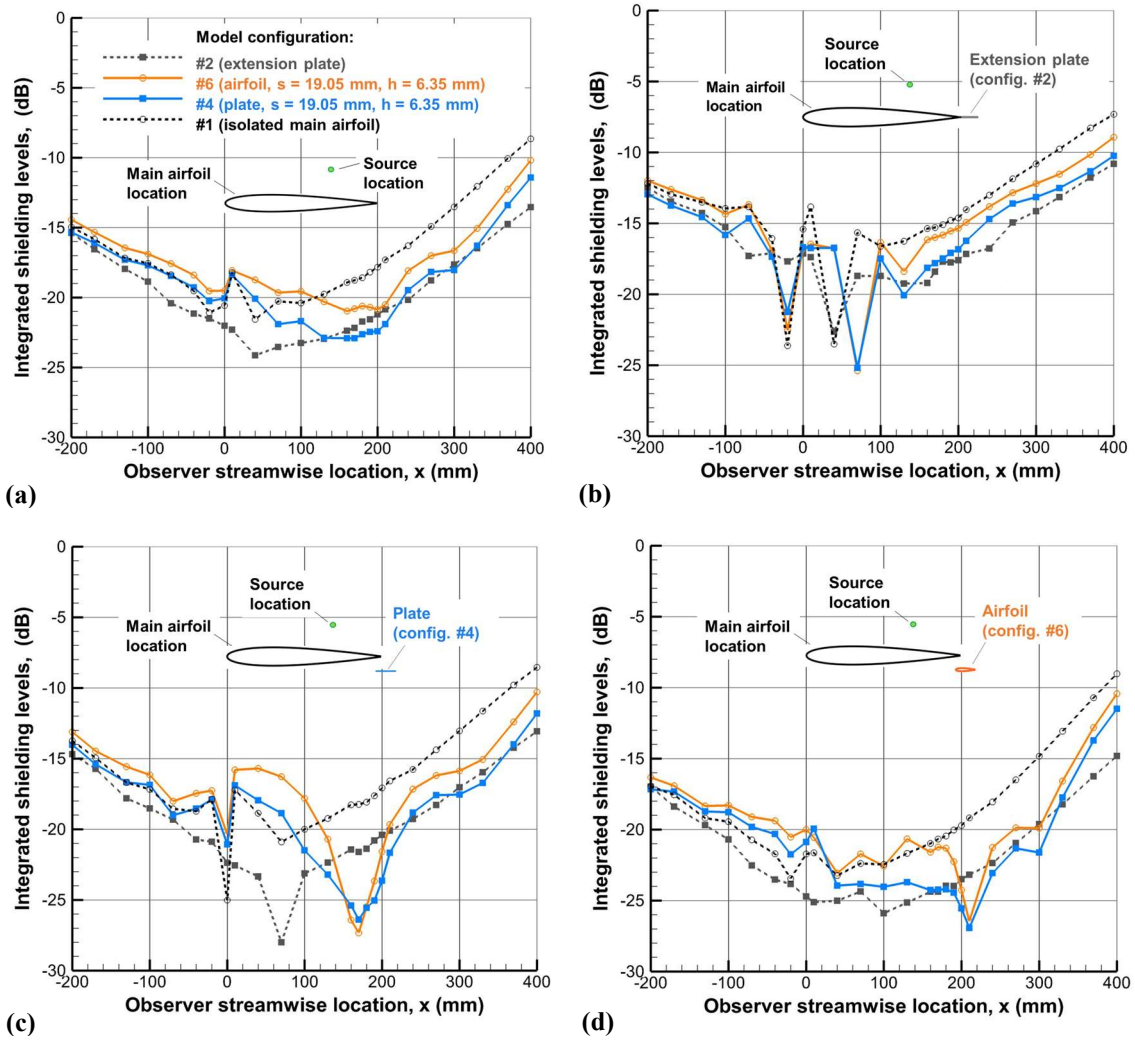

Fig. 10 Integrated shielding levels for configurations #1 (isolated main airfoil), #2 (extension plate), #4 (shifted and overhung plate) and #6 (shifted and overhung airfoil). Source at 70% chord; no flow. (a) 5 to 40 kHz; (b) 5 to 10 kHz; (c) 10 to 20 kHz; (d) 20 to 40 kHz.

The effects of changes in the flap shift and overhang on shielding are shown in Fig. 11 for the airfoil flap geometry. The integrated shielding levels obtained for configurations #6, #7 and #8 are compared to those obtained for the isolated main airfoil and extension plate cases. It is seen that reducing the shift from 19.05 mm (configuration #6) to 12.7 mm (configuration #7) and effectively narrowing the gap between the main airfoil trailing edge and the flap leads to increased shielding below the main airfoil compared to the isolated main airfoil case. Changing the flap overhang from 6.35 mm (configuration #7) to 0 (configuration #8) reverts to an increase in noise below the main airfoil. However, although individual performances vary with frequency range, all three shielding flap configurations provide added shielding benefit downstream of the main airfoil and performed better than the non-shifted (gapped) flap configurations. Overall, when considering the full frequency range, configuration #7 with the smallest shift and positive overhang performed best.

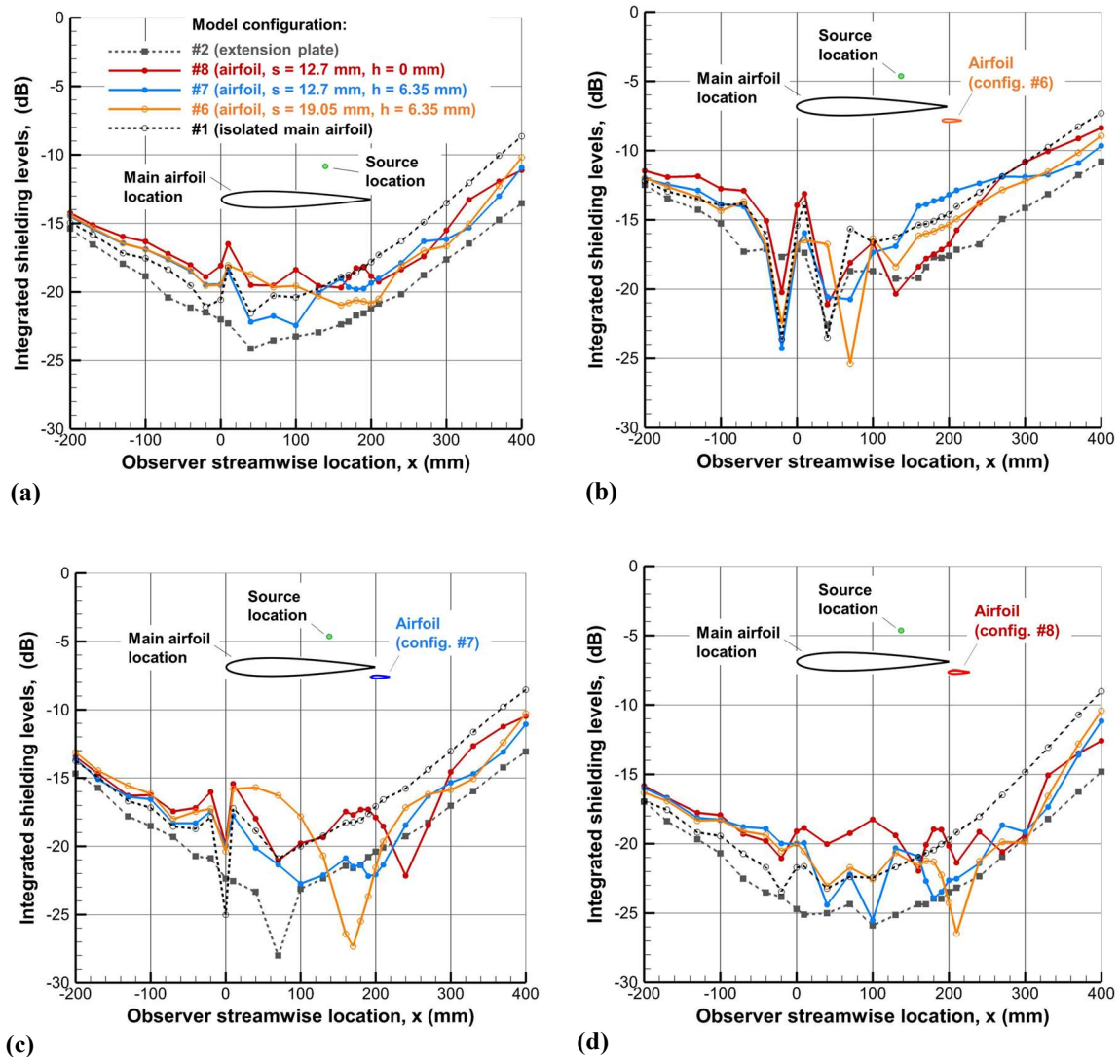

Fig. 11 Integrated shielding levels for configurations #1 (isolated main airfoil), #2 (extension plate), and #6, #7 and #8 (flaps with different shift and overhang). Source at 70% chord; no flow. (a) 5 to 40 kHz; (b) 5 to 10 kHz; (c) 10 to 20 kHz; (d) 20 to 40 kHz.

The effect of deflecting the flap trailing edge toward the main airfoil on shielding levels for the shifted airfoil cases was found to be minimal, and significant effects were only observed in the higher frequency range. The integrated shielding levels for configurations #7 and #9 (flaps with shift and overhang, without and with deflection) and configurations #8 and #10 (flaps with shift and no overhang, without and with deflection) are displayed in Fig. 12. It is seen that for either flap overhang settings, the deflection did not affect shielding levels downstream of the main airfoil significantly and only had more notable effects in the trailing edge region and below the airfoil. The most notable effects were observed for the flap with overhang (configurations #7 and #9), with a decrease in shielding seen in the leading edge region and below the main airfoil. Configuration #7 was shown in Fig. 11(a) to be the configuration

that blocked the main airfoil trailing edge diffraction and increased shielding below the airfoil the most efficiently. The decrease in shielding observed with the -10 deg deflection could be attributed to the flap surfaces redirecting more of the main airfoil trailing edge scattering through the gap and to a change in directivity of the flap leading edge scattering.

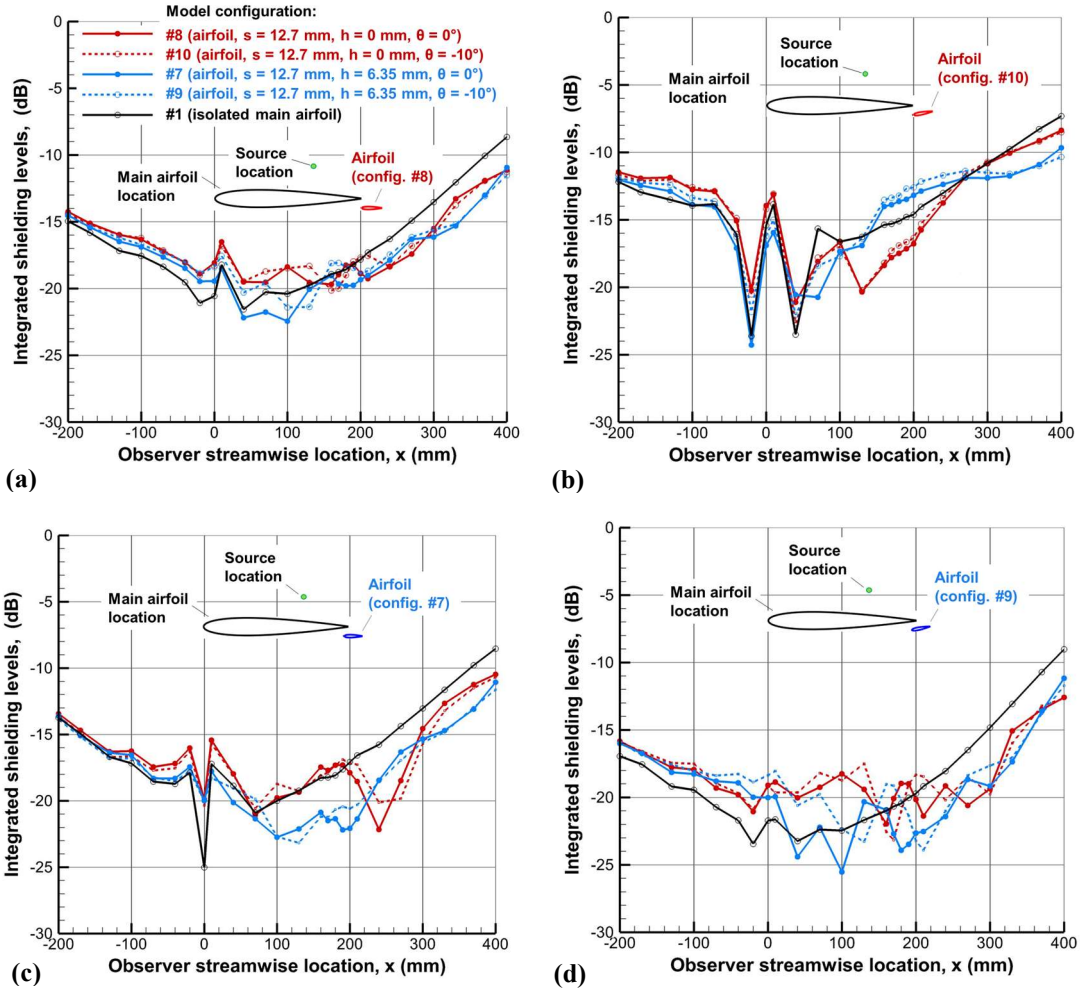

Fig. 12 Effect of shielding flap deflection. Integrated shielding levels for configurations #7 (shifted and overhung flap, no deflection), # 9 (shifted and overhung flap, -10 deg. deflection), #8 (shifted flap, no overhang, no deflection), #10 (shifted flap, no overhang, -10 deg. deflection). Source at 70% chord; no flow. (a) 5 to 40 kHz; (b) 5 to 10 kHz; (c) 10 to 20 kHz; (d) 20 to 40 kHz.

C. Effect of source location

The effect of source location on shielding is shown in Fig. 13 for a representative set of shielding flap configurations. In Fig. 13(a) the source is positioned at 75% chord (x = 150 mm) of the main airfoil and in Fig. 13(b), the source is positioned at 100% chord (x = 200 mm). In both cases, the source is located 25 mm from the airfoil surface, as opposed to 40 mm when at 70% chord as in the results presented so far. Shielding levels for the isolated main airfoil and for the extension plate cases are included for reference.

Comparing the shielding curves presented in Fig. 13(a) with those in Fig. 9(a) for the gapped flap and in Fig. 11(a) for the shifted flaps, it is seen that very similar results are obtained when moving the source from the 70% chord to the 75% chord location. When the source is positioned further downstream, at 100% chord (Fig. 13b), all flap

configurations are seen to increase shielding downstream of the midchord of the airfoil compared to the case of the isolated main airfoil. A corresponding increase in noise (decrease in shielding) is seen upstream of the midchord of the airfoil. The shielding benefit provided by the gapped flap below the main airfoil in the aft region is, however, not as high as that provided by the shifted flap configurations. Additionally, when the gap size is doubled, the shielding benefit provided by the gapped flap is replaced with a significant increase in noise in that same region (result not shown).

The effect of the addition of a shielding flap on the sound field scattered by the main airfoil is also observed to be much more pronounced when the source is located near the airfoil trailing edge than when it is located further upstream. Thus, downstream of the airfoil trailing edge, the flap blocks the otherwise direct path between the sound source and the microphones, hence the large decrease in noise in that region. Upstream of the trailing edge, the more pronounced increase in noise seen with the addition of a flap may be attributed to a strengthened contribution to the sound field of the noise scattered by the flap edges. Overall, because of the proximity of the sound source to the trailing edge of the main airfoil, a larger part of the sound field is expected to be dominated by trailing edge scattering, hence the introduction of new surfaces in that region of the airfoil is intuitively expected to have a larger impact (positive or negative) on the sound field, than for the other source locations.

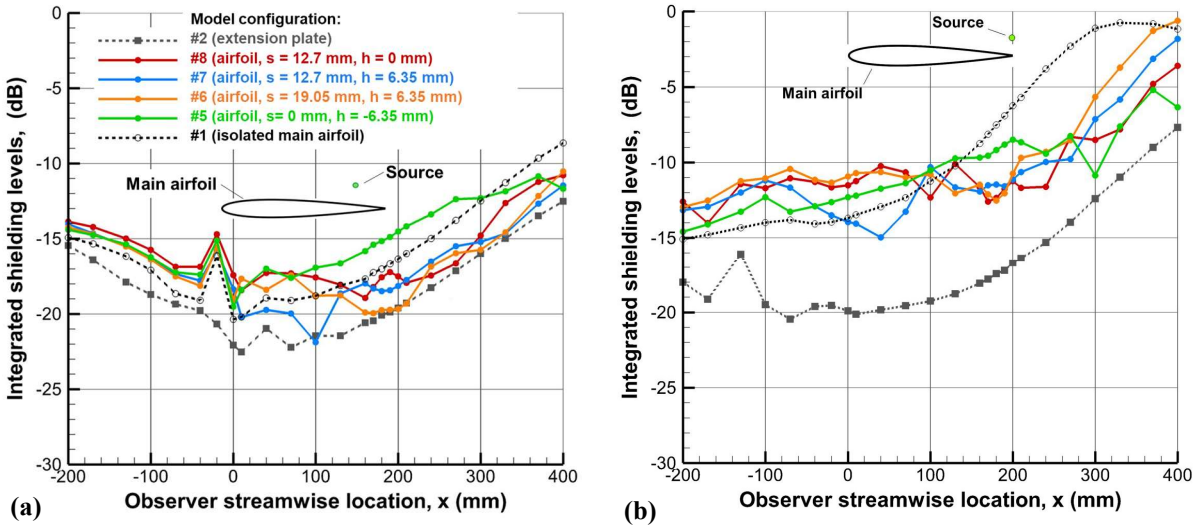

Fig. 13 Effect of source location. Integrated shielding levels for configurations #1 (isolated main airfoil), #2 (extension plate), #5 (gapped flap) and #6, #7 and #8 (flaps with different shift and overhang). Frequency range of 5 to 40 kHz; no flow. (a) Source at 75% chord; (b) source at 100% chord.

D. Effect of freestream flow

The effect of flow on the laser-induced sound source is discussed in Refs. 6 and 12. In these references, it is observed that because the source convects with the flow, a convective amplification downstream of the source and a decrease in sound upstream are observed in the presence of flow. It is also noted that this effect is most significant above 20 kHz, and little impact is apparent in the lower frequency range. However, it should be noted that Rossignol and Delfs have since pointed to the slight reversed effects (i.e., convective amplification upstream and the reverse downstream) that can be observed in the measured data at low frequencies in Refs. 6 and 12. They have noted that these reverse effects may be associated with a smearing (loss of compactness) of the sound source during heat production while it convects. These effects are successfully captured by the mathematical model of the sound source formulated by Rossignol and Delfs.[12]

The effect of flow on shielding for configurations #1, #5 and #7 is presented in Fig. 14 for a source positioned at the 70% chord location, and in Fig. 15 for a source positioned at the 100% chord location. These figures indicate that the presence of the flow significantly affects shielding levels in the highest frequency band (20 to 40 kHz), while the

levels in the two lower frequency bands only show very small variations. (This was also observed for the other flap configurations tested.) For both source locations, the presence of the flow leads to a decrease in shielding levels upstream of the main airfoil trailing edge. Although a drift in the source location and changes in the source directivity due to flow effects might also contribute, this decrease in shielding may more likely be attributed to sound refraction from the flow velocity gradient present near the model surfaces. For this effect, the sound that is scattered at the trailing edge of the airfoil (and at the edges of the flap) and traveling upstream would tend to be refracted away from the model (toward the microphones) by the mean velocity gradient of the boundary layer and shear flow. This could also explain the more pronounced flow effects that are observed for configurations #5 and #7 (as well as for the other shielding flap configurations tested), as the presence of the flap causes the airfoil boundary layer to thicken and the region of shear flow to expand, increasing refraction toward the microphones as the sound scattered from the trailing edge region propagates upstream.

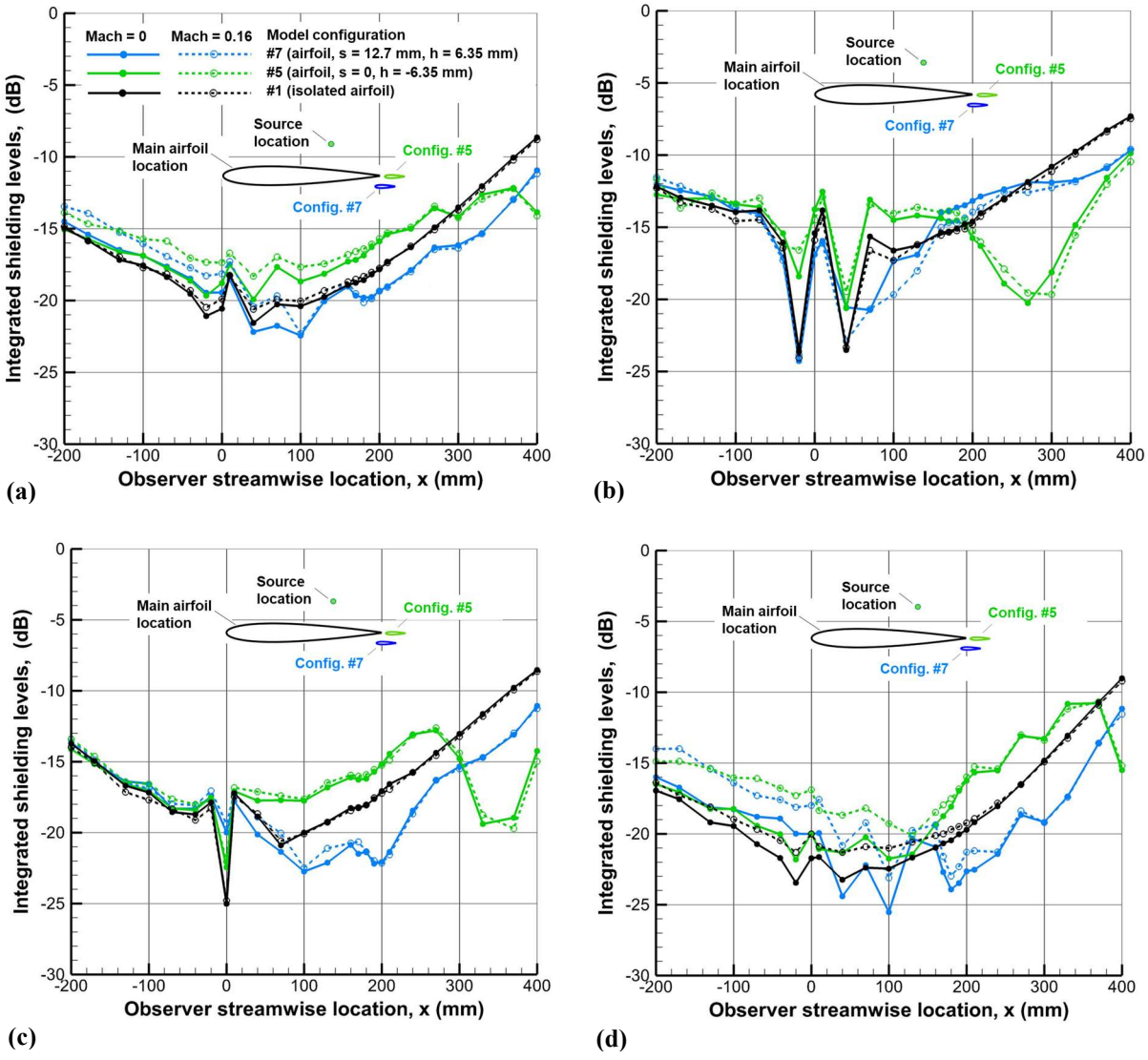

Fig. 14 Effect of Flow. Integrated shielding levels for configurations #1 (isolated main airfoil), #5 (gapped flap) and #7 (flap with shift and overhang). Source at 70% chord. (a) 5 to 40 kHz; (b) 5 to 10 kHz; (c) 10 to 20 kHz; (d) 20 to 40 kHz.

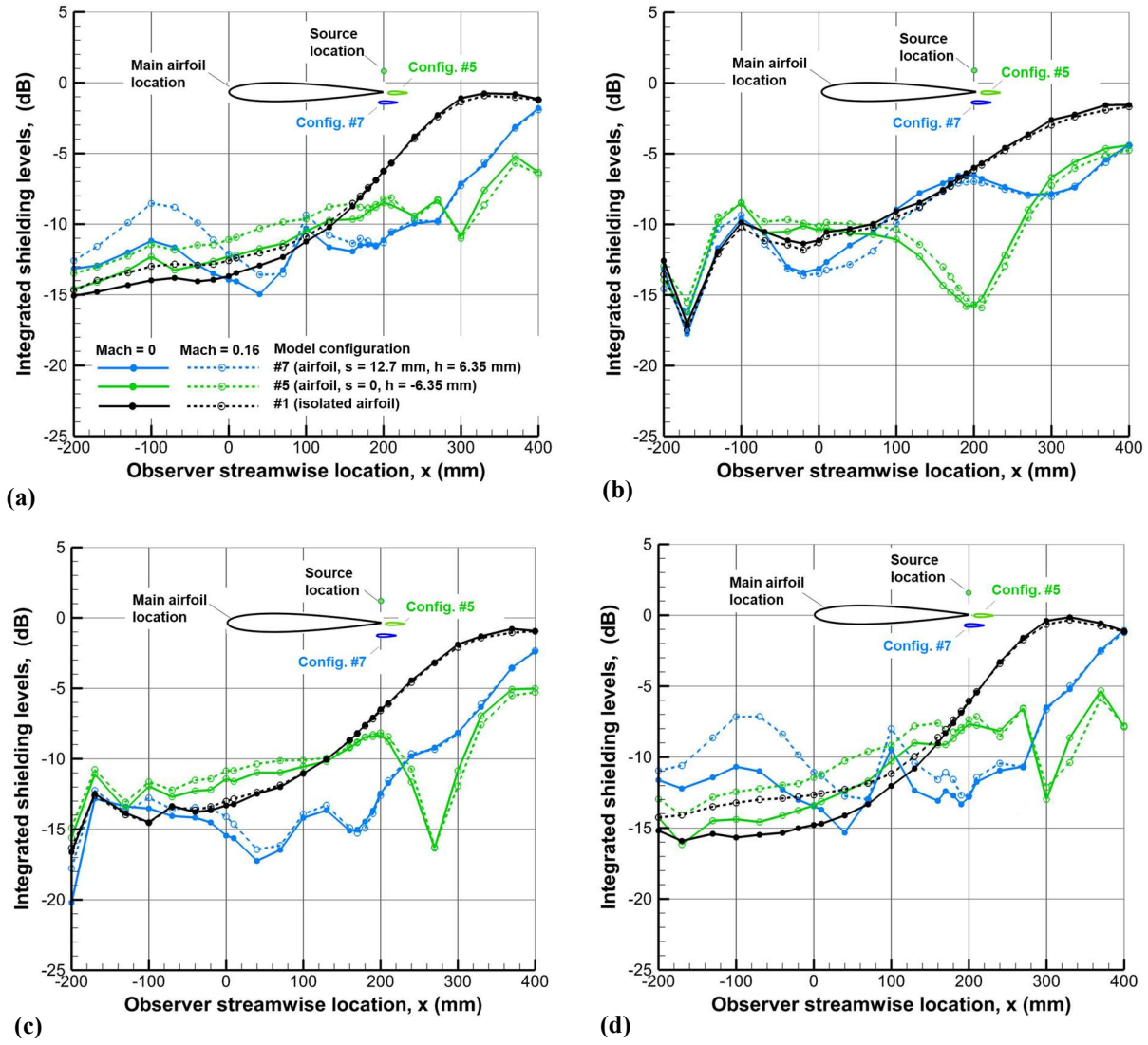

Fig. 15 Effect of Flow. Integrated shielding levels for configurations #1 (isolated main airfoil), #5 (gapped flap) and #7 (flap with shift and overhang). Source at 100% chord. (a) 5 to 40 kHz; (b) 5 to 10 kHz; (c) 10 to 20 kHz; (d) 20 to 40 kHz.

VI. Summary

A noise scattering test was performed in the NASA Quiet Flow Facility to capture the effects of a small flap on the shielding of a sound source by a NACA 0012 airfoil. Results obtained with the small flap are compared to those obtained when an extension plate is attached to the trailing edge of the NACA 0012 airfoil to capture the effects of sound leakage through the gap between the flap and airfoil. The sound source was a laser-induced plasma. The repeatability of the acoustic signal and the expected omnidirectional character of the sound produced by the plasma burst were verified. Because of the measured shielding levels' sensitivity to changes in frequency and observer location (sensitivity induced by the multipath nature of the acoustic signals), integrated shielding levels calculated over three octave bands were used to capture the general effects of the flap on shielding.

Compared to the shielding levels obtained with the isolated main airfoil, the gapped flap configurations led to decreased shielding over most observer locations, except at the most upstream locations where shielding levels approached those of the isolated main airfoil, and at the most downstream locations where shielding increased and levels could exceed those achieved in the absence of a gap (extension plate configuration). Shifting the flap toward the observers with or without an overhang led to better shielding performance than the gapped configurations, with reduced to no increase in noise below the main airfoil and shielding levels close to or better than those achieved with the extension plate in the region downstream of the airfoil midchord. Deflecting the flap trailing edge toward the main airfoil for the shifted flap configurations had minimal effects. Overall, for the range of observer locations considered in this experiment, the best shielding performance was achieved with the smallest shift and a positive overhang, a configuration where the flap shields the main airfoil trailing edge and limits sound leakage through the gap between the flap and main airfoil surfaces.

Regarding the shielding element geometry, for both the gapped and shifted configurations tested, the plate provided higher shielding levels than the airfoil; a difference in shielding performance that could be attributed to increased scattering and reflections from the airfoil's larger and curved leading edge. Note that for practical applications, the increased shielding benefit provided by the plate would be weighed against a possible loss of aerodynamic performance compared to an airfoil flap.

The installation of the flap in the trailing edge region of the main airfoil was also observed to lead to similar shielding effects on the sound field for all three source locations. These effects were, however, much more pronounced with the source located closest to the airfoil trailing edge.

Finally, the presence of flow was found to significantly affect shielding levels in the higher frequency range with a notable decrease in shielding below and upstream of the main airfoil. It is believed that this decrease in shielding is mostly due to sound refraction from the flow velocity gradient present near the model surfaces, hence the more pronounced effects observed for the flapped model configurations than for the main airfoil alone.

VII. Acknowledgments

The authors would like to gratefully acknowledge the NASA Advanced Air Transport Technology Project for supporting this work.

VIII. References

[1] Hutcheson, F. V., Brooks, T. F., Burley, C. L., Bahr, C. J., Stead, D. J., and Pope, D. S., "Shielding of Turbomachinery Broadband Noise from a Hybrid Wing Body Aircraft Configuration," AIAA paper 2014-2624, 20th AIAA/CEAS Aeroacoustics Conference, Atlanta, GA, June 16 – 20, 2014. https://doi.org/10.2514/6.2014-2624

[2] Doty, M. J., Brooks, T. F., Burley, C. L., Bahr, C. J., and Pope, D. S., "Jet Noise Shielding Provided by a Hybrid Wing Body Aircraft," AIAA paper 2014-2625, 20th AIAA/CEAS Aeroacoustics Conference, Atlanta, GA, June 16 – 20, 2014. https://doi.org/10.2514/6.2014-2625

[3] Burley, C. L., Brooks, T. F., Hutcheson, F. V., Doty, M. J., Lopes, L. V., Nickol, C. L., Vicroy, D. D., and Pope, D. S., "Noise Scaling and Community Noise Metrics for the Hybrid Wing Body Aircraft," AIAA paper 2014-2626, 20th AIAA/CEAS Aeroacoustics Conference, Atlanta, GA, June 16 – 20, 2014. https://doi.org/10.2514/6.2014-2626

[4] Rossignol, K.-S., Pott-Pollenske, M., Delfs, J., Silbermann, J., and Gomes, J. M. P., "Investigating Noise Shielding by Unconventional Aircraft Configurations," AIAA paper 2017-3195, 23rd AIAA/CEAS Aeroacoustics Conference, Denver, CO, June 5 – 9, 2017. https://doi.org/10.2514/6.2017-3195

[5] Rossignol, K.-S. and Delfs, J., "Analysis of the Noise Shielding Characteristics of a NACA0012 2D Wing," AIAA paper 2016-2795, 22nd AIAA/CEAS Aeroacoustics Conference, Lyon, France, May 30 – June 1, 2016. https://doi.org/10.2514/6.2016-2795

[6] Hutcheson, F. V., Bahr, C. J., Thomas, R. H., and Stead, D. J., "Experimental Study of Noise Shielding by a NACA 0012 Airfoil," AIAA paper 2018-2821, AIAA Aviation Forum, Atlanta, GA, June 25 – 29, 2018. https://doi.org/10.2514/6.2018-2821

[7] Clark, I. A., Guo, Y., and Thomas, R. H., "Design of an Acoustic Shielding Flap Concept with Prediction and Validation," AIAA paper 2024-3001, 30th AIAA/CEAS Aeroacoustics Conference, Rome, Italy, June 4 - 7, 2024. https://doi.org/10.2514/6.2024-3001

[8] Guo, Y. and Thomas, R. H., "Geometric Acoustics for Aircraft Noise Scattering," AIAA paper 2022-3077, 28th AIAA/CEAS Aeroacoustics Conference, Southampton, UK, June 14 – 17, 2022. https://doi.org/10.2514/6.2022-3077

[9] Hubbard, H. H. and Manning, J. C., "Aeroacoustic Research Facilities at NASA Langley Research Center: Description and Operational Characteristics," NASA Technical Memorandum 84585, 1983.

[10] Bahr, C. J., "Velocity discontinuity propagation model validation using an approximate point source in motion," *The Journal of the Acoustical Society of America*, Vol. 153, No. 5, 2023, pp. 2900 – 2908. https://doi.org/10.1121/10.0019414

[11] Guo, Y., "Diffraction by Sharp Edges of Noncanonical Shape with Mean Flow and Surface Impedance," AIAA paper 2024-3000, 30th AIAA/CEAS Aeroacoustics Conference, Rome, Italy, June 4 - 7, 2024. https://doi.org/10.2514/6.2024-3000

[12] Rossignol, K.-S. and Delfs, J., "On the Relevance of Convection Effects for a Laser-Generated Sound Source," AIAA paper 2015-3146, 21st AIAA/CEAS Aeroacoustics Conference, Dallas, TX, June 22 - 26, 2015. https://doi.org/10.2514/6.2015-3146